Traditional use of Cissampelos pareira L. for hormone disorder and fever provides molecular links of ESR1 modulation to viral inhibition

Madiha Haider[#1,2] Dhwani Dholakia[#1,2] Aleksha Panwar[5] Parth Garg[3] Vivek Anand[1,2] Atish Gheware[1,2] Khushboo Singhal[1,2] Dayanidhi Singh[1,2] Shaunak A Burse[1,2] M. Ghalib Enayathullah[6] Yash Parekh[6], Sushma Ram[6] Surekha Kumari[7,2] Anmol[7,2] Arjun Ray[3] Guruprasad R. Medigeshi[5] Kiran Kumar Bokara[6] Upendra Sharma[7,2] Bhavana Prasher[*1,2,4] Mitali Mukerji [*1,2,4]

[1]Genomics & molecular medicine, CSIR-Institute of Genomics and Integrative Biology, Delhi, India-110007, [2]Academy of Scientific and Innovative Research, Ghaziabad, Uttar Pradesh, India 201002, [3]Indraprastha Institute of Information Technology, Delhi, India 110020, [4]Centre of excellence for Applied developments of Ayurveda prakriti and genomics, CSIR's Ayurgenomics Unit TRISUTRA, CSIR-IGIB, [5]Translational Health Science and Technology Institute, Faridabad, Haryana, India 121001, [6]CSIR-Center for Cellular and Molecular Biology, Hyderabad, Telangana, 500007, India, [7]Chemical Technology Division, CSIR-Institute of Himalayan Bioresource Technology, Palampur, Himachal Pradesh 176 061, India

[*]Corresponding Authors

[#]Equal contribution by these authors

Email: mitali@igib.res.in, bhavana.p@igib.res.in

The authors declare no competing interests.

Keywords: *Cissampelos pareira* L., Ayurveda, Traditional medicine, ESR1, Dengue virus, SARS-CoV-2

Abstract:

In traditional systems, a single herbal formulation is often used in the treatment of diverse diseases, including some that are newly emergent and prevalent today. We provide here a multi-omics framework to probe the molecular basis of a multicomponent example herb, Cissampelos pareira L. (Cipa) used in the treatment of hormonal disorders and fever in Ayurveda. Cipa treated MCF7 cells exhibit downregulation of signatures of estrogen response. 38 constituent molecules in Cipa potentially bind ($\Delta G < -7.5$) with ERα at the same site as estrogen. Cipa transcriptome signatures in the connectivity map exhibit positive scores with protein translation inhibitors and knockdown signatures of genes linked to the antiviral response. This includes the knockdown signature of RPL7, a coactivator of ESRI with a connectivity score > 99.92. This axis was found to be upregulated in the COVID-19 patient transcriptome. The antiviral activity through ESR1 modulation was validated in the DENV-2 infection model. We further observed 98% inhibition of SARs-COV-2 replication in infected Vero cell cultures with the whole extract. A few of its prominent pure constituents e.g pareirarine, cissamine, magnoflorine exhibited 40-80% inhibition. This study provides a novel framework for querying the molecular links of multicomponent Ayurveda formulations and explains their use in the treatment of disparate diseases. The novel biological targets identified here can become potential that could be applicable to more than one viral infection, such as the use of Cipa in dengue and COVID-19.

Introduction:

Medicinal formulations used in Ayurveda range from single to multiple herb combinations. Besides, a single herb is used in many different disease conditions and vice versa. Multiple active principles are present in a single herb, and these components are postulated to target different pathways to bring about synergistic effects. There is a recommendation to use whole formulations instead of an herb's active principles for maximum efficacy and to minimize drug resistance that is commonly set in with a single molecule (1–3). There, however, remains a gap in understanding the molecular underpinnings of whole formulations. This has enormous utility in repurposing studies and for the therapeutic management of diseases or pathological states. Pattern matching through a common interface of connectivity map of molecular signatures of complex formulations generated in cell lines have recently gained prominence in drug repurposing studies (4). Integration of

the knowledgebase of documented use with these interfaces could provide mechanistic insights and help to uncover shared molecular pathways amongst unrelated diseases that are treated with the same herbal formulation.

Cissampelos pareira L. (Cipa) a popular herbal medicine, has been described in Ayurveda as a febrifuge (*Jwarahara*) and for balancing hormonal axis desirable in the post-partum period and for proper lactation (*stanyashodhana*) (5). It is also widely used for treating asthma, cough, skin ulcers, snakebite, and jaundice in many parts of the world (6). Alcoholic and aqueous alcoholic extracts of CIPA have antiviral and antimalarial activities, respectively (7, 8). However, there is limited research on exploring whether there are shared pathways through which these extracts work in such diverse diseases. We used an Ayurgenomics framework to explore the molecular signatures of the whole formulation of Cipa and to probe whether there are molecular players that connect the hormonal axis with antiviral inhibition.

In this study, we carried out a transcriptomic analysis of CIPA in MCF7 cell lines and queried its involvement in different pathways using gene ontology tools, Gene Set Enrichment Analysis, and probed its connectivity with drugs and other perturbagens including gene knockdowns using L1000 (9) in CMAP. Pathways linked to lipid metabolism, viral transcription, translation, and estrogen axis seem to be modulated by CIPA. It also shows a high connectivity score with protein synthesis inhibitors showing antiviral effect in *in vitro* studies. Besides the downregulation of ESR1, we also obtained a high connectivity score of Cipa with a knockdown signature of a selective estrogen receptor-alpha coactivator, RPL7 also involved in protein translation. Docking studies of CIPA constituents to estrogen receptor alpha show a high binding affinity of ~ 38 compounds to regions that bind known ERα modulators. CIPA inhibits dengue virus replication in MCF7 cell lines, and ESR1 knockdown in CIPA treated infected cells reduces this effect. RPL7 and ESR1 are significantly upregulated in BALF samples of COVID-19 patients (10, 11). A conjoint analysis of patient transcriptome signatures reveals a potential for repurposing CIPA in COVID19. This was experimentally validated in inhibition of the SARS-COV-2 in vitro by the hydro-alcoholic extract of Cipa and its pure constituents. This study, through the integration of knowledge of network medicine in Ayurveda, and provides (a) a unique framework for elucidating the molecular mechanisms of the multicomponent herbal formulation; (b) a method for prioritizing drug targets and lead compounds for repurposing; (c) biological links between diseases applicable for novel conditions.

Results:

Cipa modulates estrogen receptor alpha in MCF7 cells:

Genome wide expression assay of MCF7 cells provided 93 downregulated and 131 upregulated genes at 500µg and 253 downregulated and 587 upregulated genes at 1000µg, of Cipa treatment (**Supplementary file S1**). Gene ontology analysis revealed that the upregulated set had significant enrichment of transcription regulation by RNA polymerase II, tissue development, supramolecular fiber organization etc., whereas the downregulated genes were enriched in lipid metabolism processes (**Fig S4**).

Gene Set Enrichment Analysis (GSEA) analysis provided 59 positively and 12 negatively enriched gene sets (p-value <0.05 and FDR< 5%). We observed a significant enrichment of estrogen response gene sets in both positive and negative enrichments (**Figure 1A**). ESR1 mRNA expression was observed to be downregulated in the array that was confirmed by real-time quantitative analysis of mRNA levels in both concentrations of Cipa (**Figure 1B**). Motif searches of estrogen response elements (ERE) reveal significant enrichments in ERE density up and downregulated genes (p value= 0.0054) in the 5KB upstream region. There is no significant difference in Up regulated and unchanged genes pair and downregulated and unchanged gene pair in 5 KB upstream region (**Figure 1C**). The regression values between fold change and the number of ERE sites are given in the supplementary. Negative slope indicates that more ERE sites in the 5KB upstream region have negative effects on expression. The differentially regulated genes also include well-characterized estrogen response genes with EREs in their promoters (**Fig S5**).

To investigate the atomistic detail of possible Cipa constituent binding to the Estrogen receptor alpha, unbiased virtual screening of the constituent compounds against the receptor was employed. This revealed four preferential locations of binding for the 61 compounds. The largest cluster (pink) comprised 38 out of the 61 Cipa constituents, followed by the cluster of 8 (blue), 6 (orange), and 3 (green). As a positive control, we took previously reported SERMs, namely, tamoxifen and 17-*β*-estradiol. Our results show that both of these control molecules bind at the same location as the largest cluster in our findings with high concurrency to the reported binding energy (**Figure 2, Table 1**). Ligplot of the detailed binding sites for the controls and top binding molecules in **Fig S6**.

Connectivity map analysis reveals strong positive similarity with protein synthesis inhibitors with potential antiviral activity

A ranked gene signature of 69 down and 129 up genes was used to query the connectivity map. At a cut-off score of 95 there were 69 positively connected small compounds. The top-scoring compounds belonged to the class of protein translation inhibitors e.g., emetine (99.97), cycloheximide (99.94), verrucarin-a (99.62),

cephaeline (99.84) (**Figure 3A**). Emetine, homoharringtonine, anisomycin, cephaeline, cycloheximide, and QL-XII-47 have reported antiviral activity (**Table S2**). In the genetic perturbations set, 77 genes had knockdown (KD) signatures score >90, and all were involved in translation initiation, and viral transcription (**Figure 3B**, **Fig S7**). Since protein synthesis inhibition appears to be significant in our CMAP analysis, we decided to explore our expression data for genes involved in translation. The mRNA levels of the gene with the highest KD connectivity, RPL7 was downregulated after Cipa treatment (**Figure 3C**). In vitro assays showed moderate inhibition of translation in response to Cipa (**Fig S8**).

Cipa inhibits DENV infection in breast cancer cell lines in ESR1 dependent manner

To see whether ESR1 modulates the antiviral activity of Cipa, we infected two cell lines with varying estrogen receptor alpha expression, namely MDA MB 231 with minimal expression of ESR1 and MCF7 with higher expression of ESR1 (**Figure 4A**) with DENV-2 (**Fig S9**). Both cell lines were infected with DENV-2 at 10 MOI followed by treatment with Cipa. We found that the dengue inhibition at both concentrations of Cipa was higher than in MCF7 cells compared to MDA-MB-231 cells (**Figure 4B**). This differential inhibition could be a consequence of different cell types. Thus, to confirm that the DENV inhibition is ESR1-dependent, we performed siRNA-mediated knockdown of ESR1 in MCF7 cells. Knockdown efficiency was confirmed by qRT-PCR at 48 h post transfection which showed approximately 70-80% reduction in mRNA levels compared to that of non-targeting control (NTC) siRNA. After viral infection and subsequent Cipa treatment we observed that the inhibitory effect of Cipa was diminished in ESR1-knockdown compared to mock-treated cells suggesting that DENV inhibition due to Cipa is ESR1-dependent in MCF7 cells. (**Figure 4C, D**).

Cipa shows repurposing potential against SARS-CoV-2 as revealed by comparative analysis of patients' transcriptome

Recent studies have identified small compounds such as estrogen receptor modulators and protein translation inhibitors that could be useful against the SARS-CoV-2 infections (12), suggesting a potential repurposing potential for Cipa against the novel coronavirus.

For exploring this possibility, we compared the status of its differentially expressed genes with that of the SARS CoV-2 patients' from BALF transcriptome. We used the RNA seq data previously published (9, 10) and analyzed it in-house (**Supplementary methods**). We observed that ESR1 and RPL7, a coactivator of ESR1 were significantly upregulated in the BALF samples. The connectivity map analysis of these

transcriptomes' gene signatures and comparison with Cipa results revealed many small compounds common to both (**Table S3**). These overlaps suggest that Cipa may potentially be able to modulate the novel coronavirus.

Cipa extracts inhibit the new coronavirus *in vitro*

We tested the effect of whole and root plant extracts of Cipa in Vero cell culture assays infected with SARS-COV-2. The relative viral RNA (%) is calculated by considering the values averaged from N, ORF1ab, and E genes. The whole plant hydro-alcoholic extract (PE-50) showed a definite antiviral activity, evidenced by decreased relative viral RNA content. Results showed that at 10 μg/ml, the relative viral % concentration is ~16% and the maximum reduction to ~2% at 200 μg/ml compared with the viral control. The $\log_{10}$ viral particle was reduced to $10^{3.8}$ in the compound treated group (200 μg/ml) than the viral infection control group $10^{5.5}$ (**Figure 5B**).

The hydro-alcoholic extract from the root of Cipa (PER) also showed a reduction in relative viral RNA content. The relative viral RNA % is ~4% at 50 μg/ml and ~2% at 200 μg/ml compared with the viral control. The corresponding $\log_{10}$ viral particle of the compound treated group (200 μg/ml) showed $10^{4.1}$ compared to the viral infection of $10^{5.5}$ (**Figure 5C**). The cipa aqueous extract also shows viral reduction by 57% at 100μg/ml where the viral particle number reduced from $10^{5.9}$ to $10^{5.6}$ (**Figure 5A**).

Activity of Cipa constituents in *in vitro* inhibition of SARS-COV-2

Since we observed that certain constituents of Cipa bind estrogen receptor alpha, we wanted to see whether the Cipa pure constituents can inhibit SARS-COV-2. The total alkaloid content in the extract was 46.4 mg/g with cissamine (18.6 mg/g) being the major one, followed by magnoflorine (12.9 mg/g). The quantification of marker compounds in the root sample (USCPR-PE-R) has been reported earlier (8). The marker compounds are also quantified in the water extract (USCP-PE) (**supplementary methods, Fig S12**). **Table 2** shows the quantity of targeted molecular marker compounds in all three extracts i.e., whole plant material hydroalcoholic and aqueous extract, and the root hydroalcoholic extract.

The pure molecules namely hayatinin (US-50), salutaridine (US-DR-CP-2), cissamine (US-CP-3), Pareirarine (US-CP-5), magnoflorine (US-CP-7), PE, PE50 and PER were tested against SARS-CoV2 at 200 μM concentration showed relative viral RNA (%) to 44, 58, 45, 16, 63, 24, 2 and 2 respectively in comparison with the virus control (**Figure 6A**). The structures of these molecules are shown in **Fig. 6B**.

Discussion:

The use of *Cissampelos pareir*a in Ayurveda as a hormone balancing and antipyretic formulation is widespread, recently the antiviral activity of the formulation also came to light. Despite this, the molecular mechanisms underlying such diverse activities of Cipa remain unexplored. We built our hypothesis around the Ayurvedic knowledge of its usage and the fact that there could be possible crosstalk between the pathways implicated in these unrelated disorders, possibly through hormone response. We carried out genome-wide expression profiling of MCF7 cell lines treated with CIPA to infer their plausible mechanisms of action as well as queried the signatures in connectivity map to infer similarities with the effect of other drugs, perturbagens, and gene-knockouts.

Interestingly, the gene set enrichment analysis highlights an enrichment corresponding to the upregulation of genes upon inhibition of ESR1 and response to endocrine therapy in cancer (Figure 2A). Upon qPCR analysis, we also find a downregulation of the ESR1 mRNA by Cipa. These results suggest that Cipa may play a role as a modulator of ESR1. When we searched for the estrogen response elements in the promoter region of the genes differentially expressed by Cipa, we found that the downregulated genes were highly enriched for such elements. Excitingly, virtual screening of the constituent drug molecules against the estrogen receptor alpha revealed four distinct sites of binding. The possibility of multiple drug molecules binding at the same site shows inherent redundancy in the herbal extract. This could impart a possible beneficial role in the efficacy of Cipa and provide the synergism that is otherwise lost in isolates. The experiment also revealed an abundance of the best binding drugs which had comparable binding energies to previously reported regulatory molecules. Interestingly, magniflorine, cissamine and hyatinine were recently isolated from the hydro-ethanolic extract of Cipa shown to have antiplasmodial effect (8). These compounds are also present in the aqueous extract and have a competent binding energy with estrogen receptor alpha.

CMAP analysis has shown that the Cipa signature positively connects with protein synthesis inhibitors and the knockdown signature of genes involved in translation and ribosomal protein processing which are also enriched for viral transcription and translation. The knockdown signature of the gene RPL7, which is a large ribosomal protein 7 and is an ESR1 regulator (13) shows the highest positive connectivity with the Cipa gene signature. ESR1 is also known to regulate the immune response and estrogen regulators have been shown to possess antiviral activities (14–17). Protein translation inhibition is a very well established first-line defense against viral infections (18, 19). Recently, many translation inhibitors have been shown to possess antiviral activity and many antivirals have been found to be translation inhibitors (20, 21). All kinds of viruses have been seen to involve the endoplasmic reticulum and host translational machinery to form a membrane structure in which they reside and

replicate (22–24). Most interestingly, the biological pathways enriched for differential expression also include protein modification processes in upregulated and endoplasmic reticulum protein processing in downregulated genes. Cipa appears to inhibit translation without inducing cell death or inducing autophagy, hence proving to be an effective antiviral agent.

Our results so far indicate an involvement of the estrogen axis in the antiviral activity of Cipa. Upon experimental validation we observed that Cipa induced reduction of viral titers was markedly lower in MDA-MB-231 cells which are naturally deficient in estrogen receptor alpha and also in MCF cells when ESR1 gene is knocked down. Thus, signifying the effect of the estrogen axis in the antiviral action.

During our study, the pandemic SARS-CoV-2 has broken out and a lot of studies done on coronaviruses have come to light. Interestingly, one of the studies on coronavirus done after the SARS, MERS breakout (25) has shown estrogen receptor inhibitors and protein translation inhibitors to have potential inhibitory activity. Based on our results, Cipa appears to be both, a moderate protein synthesis inhibitor and an estrogen receptor modulator. Many of the drugs positively connected with Cipa have been reported to be a potential antiviral agent. Drugs such as emetine and homoharringtonine, which show the highest positive connectivity with Cipa have even been reported to possess potential antiviral activity against SARS-CoV-2 (26–29).

The meta-analysis of SARS-CoV-2 patients BALF transcriptome shows that there is an enrichment of pathways corresponding to protein processing and endoplasmic reticulum, protein targeting to ER, etc. in BALF, which are downregulated by Cipa. Moreover, RPL7 and ESR1 which are upregulated in BALF are downregulated by Cipa. Our analyses comparing the gene expression signatures of BALF with those of Cipa show overlaps which are central for the antiviral activity of a therapeutic. Strikingly, in vitro studies have shown that Cipa can potentially inhibit SARS-CoV-2. Both the whole plant extracts and single chemical compounds of Cipa have shown marked inhibition of SARS cov-2 in vitro.

Our analysis, based on the insight from Ayurvedic knowledge, seems to have opened a large number of questions regarding the role of estrogen receptors in antiviral activity. That a gender bias in immune response exists is well-known (30). Gender differences, estrogen receptor modulators and signaling pathways have been observed in various studies on the novel coronavirus 2019 (31, 32). Direct evidence of gender bias in the outcomes of coronavirus infections have also been reported (33). Our study suggests that this hormone balancing Ayurvedic formulation can be considered as a potential antiviral defense strategy against the novel coronavirus. It will be interesting to study these pathways in detail in the context of virus infections.

Conclusion:

This study provides a novel framework for prioritizing Ayurvedic formulations for drug repurposing and discovery of bioactive/small molecules by integrating Ayurvedic knowledge with the transcriptomic approach to generate characteristic gene expression signatures. Such an approach can also be utilized for varied as well as novel diseases such as the recent pandemic.

Materials and methods:

Cell culture and Cipa treatment:

Cissampelos pareira whole plant extract was obtained commercially in lyophilized form, from a GMP certified manufacturer. Crude water extracts were reconstructed from powdered Cipa. Fresh extracts were prepared right before each experiment.

MCF7 (triple positive breast cancer) cell line was obtained from NCCS, Pune. It was maintained in DMEM high glucose media, supplemented with 10% FBS,1M HEPES and 1X antibiotic antimycotics. The cells were kept at 37˚C and 5% CO_2. MycoAlert (Cat no. LT07-318) was used to test the culture for mycoplasma.

MCF7 cells were treated with 1µg, 10µg, 100µg, 500µg and 1000µg per ml of the aqueous extract from *Cissampelos pareira* L. The extract was prepared outside the cell culture hood and then filtered using 0.22µm syringe filter before its use in cell culture. The MCF7 cells were seeded at a confluency of 60-70% 18-24 hrs. prior to treatment. The cells were treated with Cipa for 24 hours for each experiment. A fresh extract was made for each set of experiments.

RNA isolation and Whole transcriptome analysis:

MCF-7 cells were seeded in 6 well plates at 60-65% confluency and then treated with vehicle, 1µg, 10µg, 100µg, 500µg and 1000µg of Cipa for 24 hours. The cells were then trypsinized and washed with PBS. Total RNA was isolated using TRIzol (Ambion, Cat no. 15596026) extraction method and its integrity was checked on 1% agarose gel which was followed by Nanodrop quantification (ND1000, Nanodrop technologies, USA). Genome-wide transcriptome data was generated using 250µg of the total RNA for each sample following the manufacturer's protocol. GeneChip™ (Affymetrix) Human Transcriptome Array 2.0 cartridges were used for this experiment. HTA 2.0 chip can capture 245,349 protein coding transcripts and 40,914 non protein coding transcripts in a 64-format. Briefly, the total RNA was prepared with poly A controls and first strand cDNA followed by second strand cDNA were synthesized. This was followed by in vitro transcription to form cRNA which was used as a template for the formation of single strand cDNA or ss-cDNA. Finally, the ss-cDNA was fragmented and

labelled. At each step, purification and quantification of the samples were ensured. Approximately 200µl of the sample, containing about 5.2µg of the labelled ss-cDNA was loaded into the cartridges, which were then kept in the Affymetrix® Hybridization Oven, set at 45°C and RPM 60, overnight. The cartridges were registered on AGCC (Affymetrix® GeneChip® Command Console) and the fluidics of the experiment (washing and staining) was done using Affymetrix® GeneChip® Fluidics Station 450. The stained chips were then scanned using GeneChip™ Scanner 3000. The preliminary images were quality checked and .cell files were generated.

The generated CEL files were background normalized using the RMA method. Batch effects were removed and differential gene expression analysis was done using the limma package in R. After background correction and RMA normalization, the probes that exceeded the p value<0.05 were annotated and analyzed for differential expression. Since no probe could qualify the cut off at 1µg, 10µg and 100µg, the differential gene expression was calculated using the dataset from 500µg and 1000µg treatments with the vehicle used as control. The raw files and data have been submitted to GEO with the accession number GSE156445.

Functional enrichment of the differentially expressed genes:

For functional analysis we used g: profiler (34) (https://biit.cs.ut.ee/gprofiler/gost). After correcting for FDR<5%, enrichments were analyzed for GO: Molecular Function, Cellular Compartment, Biological Processes, KEGG and Reactome.

In order to identify the specific sets of genes modulated by Cipa, we used Gene set enrichment analysis. We carried out a pre-ranked analysis for GSEA, in which the gene list was ordered from the highest positive gene expression to the lowest negative gene expression. The latest versions of gene sets databases were selected for query. Datasets with more than 500 and less than 15 genes were excluded from the query. The output was set to a minimum cut off of p value<0.05 and corrected for FDR<25%. An additional filter of FDR<5% was applied for identification of significant enrichments.

ERE analysis:

Sequence of 5KB upstream region of genes were downloaded from UCSC genome browser for Human genome GRCh38 build. ERE sites were mapped to 5KB upstream sequence using promo tool (33) with similarity cut off value of 8.7. High ERE density in 5KB upstream leads to down regulation of genes as per regression analysis. ERE density's coefficient of slope of regressed line (β = -0.0044) is negative and p-value is significant (0.018). Pair wise ERE density comparison of differentially expressed genes and unchanged genes was done using R software (version 3.2).

Virtual screening of constituent compounds for estrogen receptor binding affinity:

Virtual screening of CIPA ligands was performed against the estrogen receptor crystal structure (PDBID: 3OS8) using Autodock Vina, a more accurate and faster version of Autodock 4. The CIPA ligands available in the PubChem database were downloaded from there, the 3D structures of the rest of the ligands were drawn using Marvin Sketch, a computational tool for drawing 3 and 2 dimensional chemical structures. The structures were randomized and minimized prior to docking. A blind docking study was performed for each ligand wherein the possible search-space was the complete receptor molecule. For each drug molecules, the docking parameters were as follows: center_x: 9.43, center_y: 22.811, center_z : 23.418, size_x: 60, size_y: 60, size_z: 60, exhaustiveness 5000, num_modes 50000, energy_range: 20. Furthermore, for each ligand, 50 such runs were performed and the conformation with the minimum binding energy from among all the stable conformations of the 50 runs (a total of 1000 conformational possibilities) was selected for the cluster analysis.

The analysis was performed using ADT, UCSF Chimera and LigPlot+.

Connectivity map analysis for identifying similarities with known perturbations:

The connectivity map dataset currently contains 1,319,138 gene expression profiles, resulting in 473,647 signatures, generated against approximately 27,000 perturbations in 9 cell lines including MCF7, HEPG2, A549, A375, PC3, HCC515, HT29, HA1E and VCAP. The differentially expressed genes were ranked according to fold change and a signature of up and downregulated genes was generated. The gene signature containing genes which were valid i.e., having a valid HGNC symbol or Entrez ID and were also present in the LINCS gene space (represented in the L1000 data as landmark or well inferred) was used to query the connectivity map using clue.io touchstone database.

Cipa treatment in DENV infection:

MCF-7 were seeded at 100,000 cells per well in 24 well plate and were maintained for 24 hours (37 degrees; 5% CO2). Virus challenge (at 10 MOI, see supplementary) was given for 1 hour, here the media was supplemented with 2% FBS. After 1-hour of viral adsorption, cells were washed with PBS and DMEM high glucose with 10% FBS with or without Cipa (50µg and 100µg) was added. DENV titers in the supernatant were determined by plaque assay at 24 h pi. DENV plaque assay was set up in BHK-21 cells. 50,000 BHK-21 cells were plated per well in 24-well plate. Serial dilutions of virus were added in triplicates and allowed to adsorb for 1 h, followed by overlay with 0.5% carboxymethyl-cellulose (CMC; Sigma). After 72 h, cells were fixed in 3.7% formalin and plaques were visualized by staining with crystal violet.

siRNA-mediated knockdown of ESR1 in MCF7 cells:

1 μM concentration of siRNA targeting ESR1 gene and non-targeting control (NTC) were mixed with Opti-MEM (Life Technologies) and 1 μl of Lipofectamine RNAiMax to a total volume of 100 μl in a 24-well plate. Cells were trypsinized and volume made up so as to contain 60,000 cells in 400 μl antibiotic-free medium. After 20 min incubation of the transfection complex, cell suspension was added into each well. Knockdown efficiency was determined by qRT-PCR at 48 h post transfection. Cells were infected with DENV-2 at 48 h post transfection. Cipa was added at a concentration of 50 μg after 1 h of viral adsorption. DENV titers were measured by plaque assay at 24 h pi.

Cell culture, viral infection and drug treatment for inhibition of SARS-COV-2 by Cipa:

The effect of PE50 and PER was tested against the SARS-CoV2 (35) in a 96-well tissue culture plates that was seeded with Vero Cells 24 h prior to infection with SARS-CoV2 (Indian/a3i clade/2020 isolate) in BSL3 facility. The cells were maintained in Dulbecco Minimum Essential Medium (DMEM) (Gibco) containing 10% Fetal Bovine Serum (FBS) (Gibco) at 37°C, 5% CO2. Initially the compounds were dissolved in organic and aqueous solvents based on the requirements, and stocks were made. The concentrations (200, 100, 50, 10, 5 (μg/mL), were made using the DMEM media. Briefly, the cells were pre-incubated with the compounds (PE-50 & R) for 2 hours, for each concentration in triplicate. Later, the virus inoculum (at a 0.1 MOI) was added to the cells for 3 hours in presence of the respective dilutions of compounds made in Basal medium only. Post-infection, viral inoculum was replaced with fresh media containing 10% FBS and the experiment is continued in the presence of different dilutions of compounds for 72 hours. After 72 hours, cell supernatant was collected and spun for 10 min at 6,000 g to remove debris and the supernatant was transferred to fresh collection tubes for further analysis.

Isolation of Viral RNA:

RNA was isolated from 200 μL of the supernatants using the MagMAXTM Viral/Pathogen Extraction Kit (Applied Biosystems, Thermofisher) according to the manufacturer's instructions. The viral supernatants from the test groups were added into the deep well plate (KingFisherTM Thermo Scientific) along with a lysis buffer containing the following components - MagMAXTM Viral/Pathogen Binding Solution (260μL); MVP-II Binding Beads (10 μL); MagMAXTM Viral /Pathogen Proteinase-K of (5 μL) respectively. RNA extraction was performed using KingFisher Flex (version 1.01, Thermo Scientific) by following manufacturer's instructions. The eluted RNA was immediately stored in -80^{0}C until further use.

TaqMan Real-time RT-PCR assay for Detection of SARS-CoV-2:

The detection of genes specific to SARS-CoV2 was done using COVID-19 RT-qPCR Detection Kit (Fosun 2019-nCoV qPCR, Shanghai Fosun Long March Medical Science

Co. Ltd.) according to the manufacturer's instructions. The kit detects Envelope gene (E; ROX labelled), Nucleocapsid gene (N- JOE labelled) and open reading frame 1ab (ORF1ab, FAM labelled) specific to SARS-CoV2 for detection and amplification of the cDNA. Briefly, RT-qPCR assays were performed on a Quant studio Q5 (Thermo fisher). A 10 µL of Negative Control, 10 µL of Positive Control (positive and negative controls were provided by kit), and 10 µL of extracted RNA from samples were added in different PCR reaction tubes. The contents were centrifuged at low speed. The cycling conditions are: Step 1: 50°C for 15 minutes, 1 cycle; Step 2: 95°C for 3 minutes, 1 cycle; Step 3: 95°C for 5 seconds to 60°C for 40 seconds, 5 cycles; Step 4: 95°C for 5 seconds to 60°C for 40 seconds, 40 cycles. The signals of FAM, JOE, ROX and CY5 (internal reference) fluorescence channels were collected at 60°C. SARS-CoV-2 cDNA (Ct~28) was used as a positive control. The log viral particles and a semi–log graph was plotted using Graph Pad Prism 5 software (ver 5.03). The calculations for the relative viral RNA content and log reduced viral particles was calculated using the linear regression equation obtained using the RNA extracted from the known viral particles by RT-qPCR, using N, E and ORF1ab genes specific to SARS CoV2 virus. from the test samples (36).

Declarations:

Acknowledgments:

The authors would like to thank Mr. Manish Kumar for imaging facility, Dr. TN Vivek for critical inputs, Himanshi Tanwar, Ratika Sehgal and Shivam Singh for technical support. The authors acknowledge Dr. Rakesh Mishra (director-CCMB) for facilitating and support for SARS-CoV-2 infection model. The authors acknowledge Council of Scientific Research (CSIR) TRISUTRA (MLP-901) and Center of Excellence on Applied Developments in Ayurveda, Prakriti and Genomics, grant by Ministry of AYUSH (GAP0183), Govt. of India for funding the project. Research fellowship support to MH (University Grants Commission), DD (Department of Biotechnology) SK (CSIR) and Anmol (DST-INSPIRE) is duly acknowledged.

Authors' Contributions:

Conceived the study: MM and BP

Designed the study: MM, BP, MH, DD

Performed experiment: MH, AP, VA, AG, KS, DS, S.A.B, M.G.E, YP, SR, SK, A

Resources from Ayurveda: *BP

Connectivity map: MH, DD, BP, *MM

Transcriptome: MH, DD, *MM

Functional validations: MH, DS, KS

Molecular Docking: PG, *AR

Dengue infection model: AP, AG, *G.R.M

Characterization, isolation of molecules: SK, A, *US

SARS-CoV2 infection model: M.G.E, Y.P, S.R, *K.K.B

Data Synthesis and Analysis: MH, DD, *BP, *MM,

Wrote the manuscript: MH, DD, BP, MM,

*Project Leads

Ethics approval statement

The Anti-SARS CoV2 study was approved from Institutional Bio-safety Committee of CSIR-Center for Cellular and Molecular Biology, Hyderabad, India.

References:

1. N. Sehgal, *et al.*, Withania somnifera reverses Alzheimer's disease pathology by enhancing low-density lipoprotein receptor-related protein in liver. *Proc. Natl. Acad. Sci.* **109**, 3510–3515 (2012).

2. M. A. Elfawal, M. J. Towler, N. G. Reich, P. J. Weathers, S. M. Rich, Dried whole-plant Artemisia annua slows evolution of malaria drug resistance and overcomes resistance to artemisinin. *Proc. Natl. Acad. Sci. U. S. A.* **112**, 821–6 (2015).

3. B. Patwardhan, R. A. Mashelkar, Traditional medicine-inspired approaches to drug discovery: can Ayurveda show the way forward? *Drug Discov. Today* **14**, 804–811 (2009).

4. J. Lamb, *et al.*, The Connectivity Map: Using Gene-Expression Signatures to Connect Small Molecules, Genes, and Disease. *Science (80-.).* **313**, 1929–1935 (2006).

5. S. Singh, K. Nishteswar, B. Patel, Therapeutic efficacy of Patha (Cissampelos pareira Linn.) - A Review through classical texts of Ayurveda. *J. Ayurveda Integr. Med.* **1**, 92–110 (2016).

6. D. K. Semwal, R. B. Semwal, I. Vermaak, A. Viljoen, From arrow poison to herbal medicine--the ethnobotanical, phytochemical and pharmacological significance of Cissampelos (Menispermaceae). *J. Ethnopharmacol.* **155**, 1011–1028 (2014).

7. R. Sood, *et al.*, Cissampelos pareira Linn: Natural Source of Potent Antiviral Activity against All Four Dengue Virus Serotypes. *PLoS Negl. Trop. Dis.* **9**, 1–20 (2015).

8. V. Bhatt, *et al.*, Chemical profiling and quantification of potential active constituents responsible for the antiplasmodial activity of Cissampelos pareira. *J. Ethnopharmacol.* **262**, 113185 (2020).

9. A. Subramanian, *et al.*, A Next Generation Connectivity Map: L1000 Platform and the First 1,000,000 Profiles. *Cell* (2017) https:/doi.org/10.1016/j.cell.2017.10.049.

10. Y. Xiong, *et al.*, Transcriptomic characteristics of bronchoalveolar lavage fluid and peripheral blood mononuclear cells in COVID-19 patients. *Emerg. Microbes Infect.* **9**, 761–770 (2020).

11. Z. Zhou, *et al.*, Heightened Innate Immune Responses in the Respiratory Tract of COVID-19 Patients. *Cell Host Microbe* **27**, 883-890.e2 (2020).

12. D. E. Gordon, *et al.*, A SARS-CoV-2 protein interaction map reveals targets for drug repurposing. *Nature* (2020) https:/doi.org/10.1038/s41586-020-2286-9.

13. K. A. Duncan, P. Jimenez, L. L. Carruth, The selective estrogen receptor-alpha coactivator, RPL7, and sexual differentiation of the songbird brain. *Psychoneuroendocrinology* **34**, 30–38 (2009).

14. S. Kovats, Estrogen receptors regulate innate immune cells and signaling pathways. *Cell. Immunol.* **294**, 63–69 (2015).

15. K. Watashi, *et al.*, Anti-hepatitis C virus activity of tamoxifen reveals the functional association of estrogen receptor with viral RNA polymerase NS5B. *J. Biol. Chem.* **282**, 32765–32772 (2007).

16. G. Deng, *et al.*, Association of estrogen receptor α polymorphisms with susceptibility to chronic hepatitis B virus infection. *Hepatology* **40**, 318–326 (2004).

17. D. Tohma, *et al.*, An estrogen antagonist, cyclofenil, has anti-dengue-virus activity. *Arch. Virol.* **164**, 225–234 (2019).

18. C. McCormick, D. A. Khaperskyy, Translation inhibition and stress granules in the antiviral immune response. *Nat. Rev. Immunol.* **17**, 647–660 (2017).

19. A. Dalet, E. Gatti, P. Pierre, Integration of PKR-dependent translation inhibition with innate immunity is required for a coordinated anti-viral response. *FEBS Lett.* **589**, 1539–1545 (2015).

20. J. Su Yin Low, K. Caiyun Chen, K. Xing Wu, M. Mah-Lee Ng, J. Jang Hann Chu, Antiviral Activity of Emetine Dihydrochloride Against Dengue Virus Infection. *J. Antivir. Antiretrovir.* **01**, 062–071 (2009).

21. A. L. C. Valadão, *et al.*, Natural plant alkaloid (Emetine) inhibits HIV-1 replication by interfering with reverse transcriptase activity. *Molecules* **20**, 11474–11489 (2015).

22. I. Romero-Brey, R. Bartenschlager, Endoplasmic reticulum: The favorite intracellular niche for viral replication and assembly. *Viruses* **8**, 1–26 (2016).

23. P. V'kovski, *et al.*, Determination of host proteins composing the microenvironment of coronavirus replicase complexes by proximity-labeling. *Elife* **8**, 1–30 (2019).

24. V. Más, J. A. Melero, Entry of enveloped viruses into host cells: membrane fusion. *Subcell. Biochem.* **68**, 467–487 (2013).

25. J. Dyall, *et al.*, Repurposing of clinically developed drugs for treatment of Middle East respiratory syndrome coronavirus infection. *Antimicrob. Agents Chemother.* **58**, 4885–4893 (2014).

26. L. Shen, *et al.*, High-Throughput Screening and Identification of Potent Broad-Spectrum Inhibitors of Coronaviruses. *J. Virol.* **93** (2019).

27. J. Cao, J. Forrest, X. Zhang, A Screen of the NIH Clinical Collection Small Molecule Library Identifies Potential Anti-Coronavirus Drugs. *Antiviral Res.* **114** (2014).

28. R. Yu, L. Chen, R. Lan, R. Shen, P. Li, Computational screening of antagonists against the SARS-CoV-2 (COVID-19) coronavirus by molecular docking. *Int. J. Antimicrob. Agents* **56**, 106012 (2020).

29. S. Yang, *et al.*, Emetine inhibits Zika and Ebola virus infections through two molecular mechanisms: inhibiting viral replication and decreasing viral entry. *Cell Discov.* **4**, 31 (2018).

30. S. L. Klein, K. L. Flanagan, Sex differences in immune responses. *Nat. Rev. Immunol.* **16**, 626–638 (2016).

31. S. Micholas, S. Jeremy C., Repurposing Therapeutics for COVID-19: Supercomputer-Based Docking to the SARS-CoV-2 Viral Spike Protein and Viral Spike Protein-Human ACE2 Interface. *chemRxiv* (2020) https:/doi.org/10.26434/chemrxiv.11871402.v4.

32. G. Sharma, A. S. Volgman, E. D. Michos, Sex Differences in Mortality From COVID-19 Pandemic. *JACC Case Reports* (2020) https:/doi.org/10.1016/j.jaccas.2020.04.027.

33. R. Channappanavar, *et al.*, Sex-based differences in susceptibility to SARS-CoV infection. *J. Immunol.* **198**, 319–335 (2018).

34. U. Raudvere, *et al.*, g:Profiler: a web server for functional enrichment analysis and conversions of gene lists (2019 update). *Nucleic Acids Res.* **47**, W191–W198 (2019).

35. ASTM, Standard Test Method to Assess the Activity of Microbicides against Viruses in. *Astm* (2015).

36. L. Caly, J. D. Druce, M. G. Catton, D. A. Jans, K. M. Wagstaff, The FDA-approved drug ivermectin inhibits the replication of SARS-CoV-2 in vitro. *Antiviral Res.* (2020) https:/doi.org/10.1016/j.antiviral.2020.104787.

Figures and Tables:

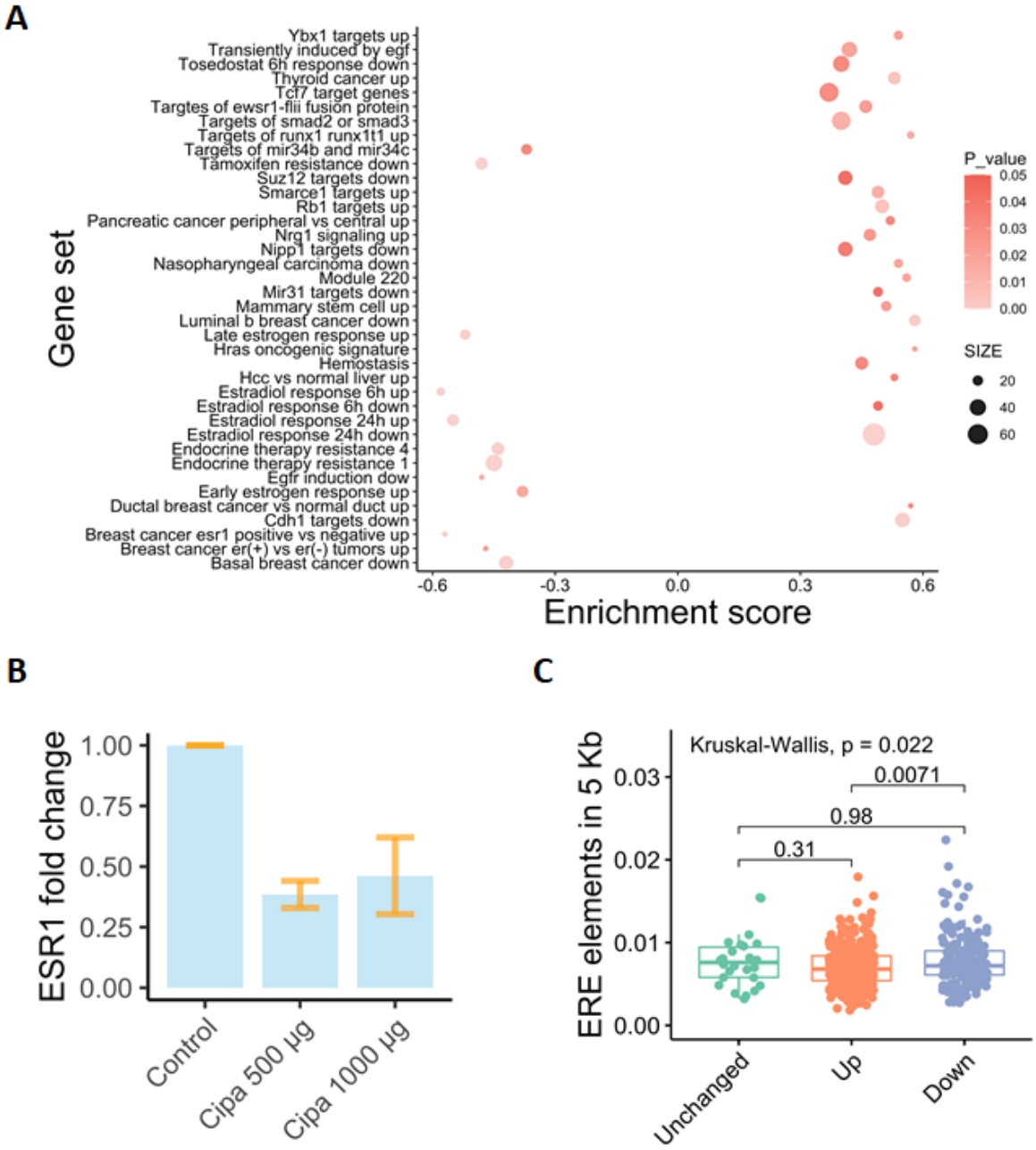

Figure 1: Estrogen receptor modulation by Cissampelos pareira: A) Gene sets enriched for genes differentially expressed, positive enrichment score for upregulated and negative score for downregulated genes. p-value <0.05 and FDR< 5%. B) Fold change in mRNA expression of ESR1 transcript at 500 and 1000µg. *** p-value<0.001, ** p-value<0.01. C) Density of estrogen response elements 5Kb upstream of differentially expressed genes, the ERE elements are higher in density in down regulated genes than upregulated genes (p value<0.05).

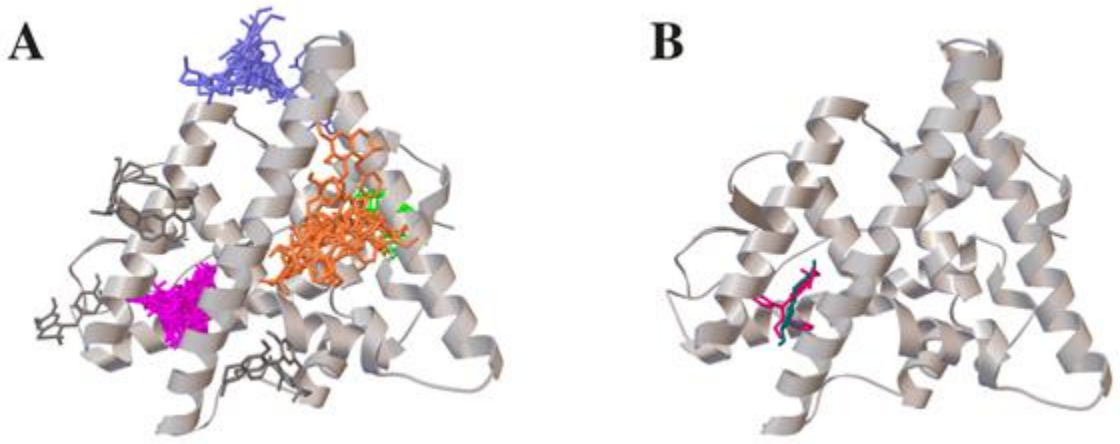

Figure 2: Plot for virtual docking sites of 61 Cipa constituents (four clusters, pink, green, orange and blue) and binding site of tamoxifen (pink) and 17 beta estradiol (blue) on estrogen receptor alpha.

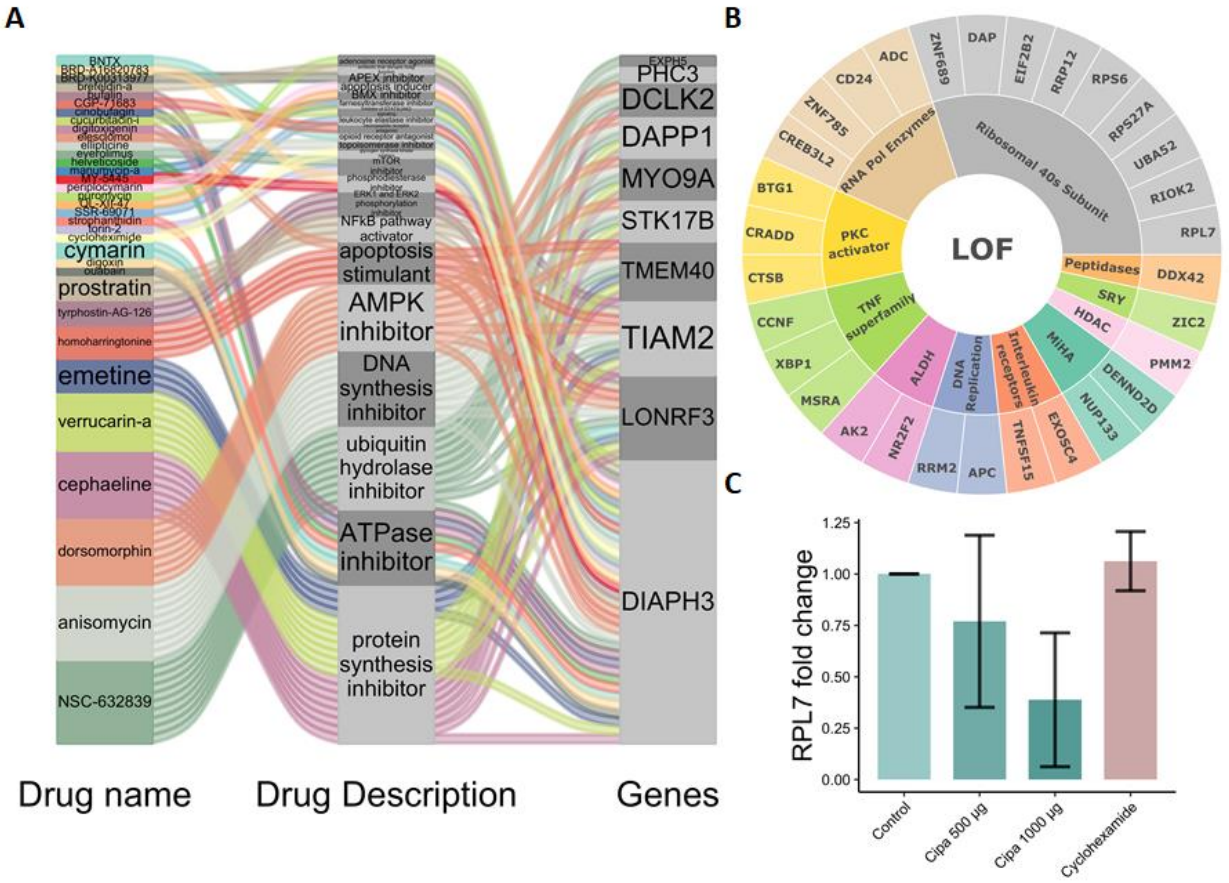

Figure 3: Connectivity map analysis of Cipa gene expression signature: A) Alluvial plot depicts small compounds with highest connectivity score >99, the class of perturbation they belong to such as protein synthesis inhibitor and the genes common with the signatures. B) Sunburst diagram shows the frequency of 11 perturbation types to which the top 30 loss of function signatures belong. C) mRNA expression of RPL7 gene in response to Cipa, *** p-value<0.001

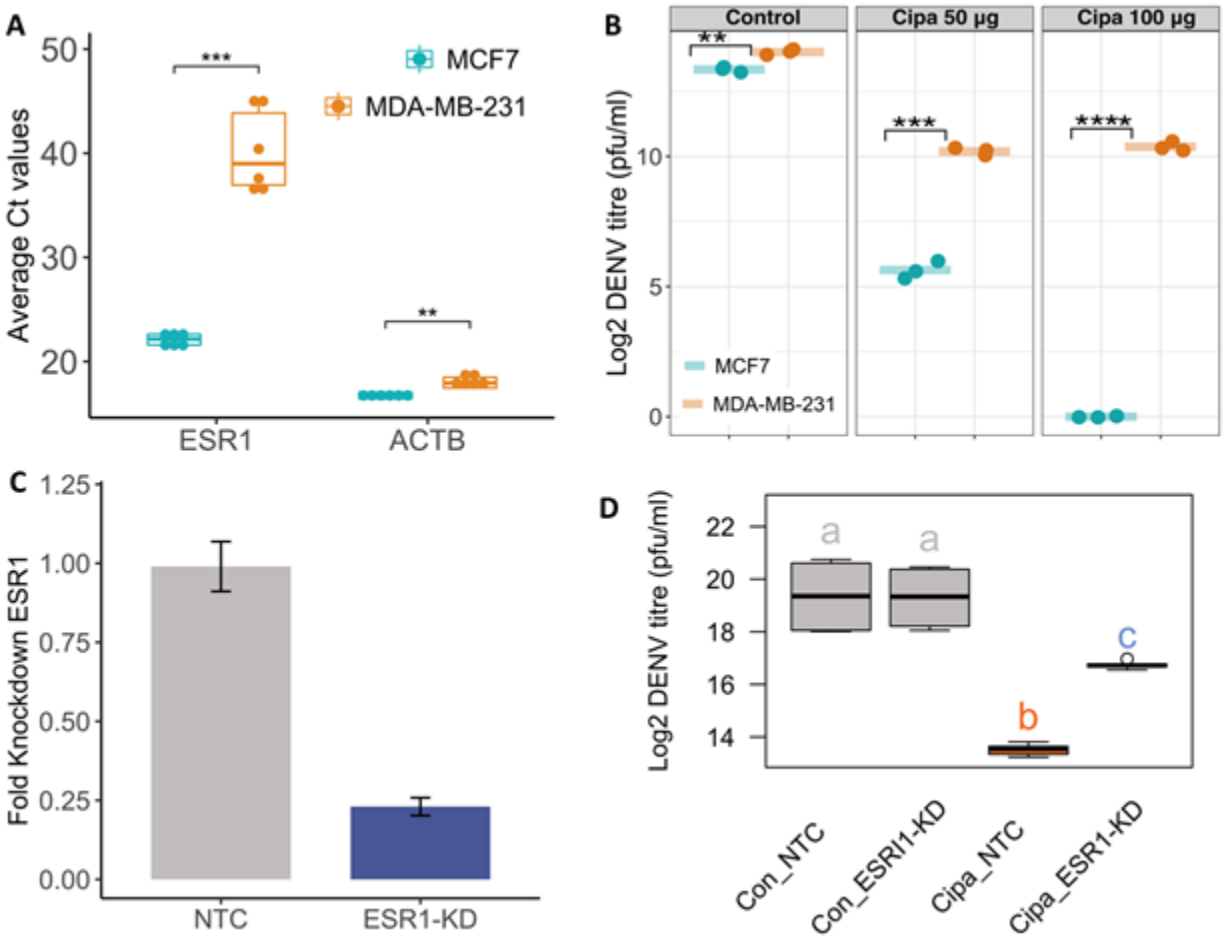

Figure 4: DENV inhibition by Cipa in ESR1-dependent manner: A) Average Ct value of ESR1 and ACTB in MCF7 and MDA-MB-231 cells. Both cell lines were infected with DENV at 10 MOI and after viral adsorption, Cipa was added at two different concentrations of 50 and 100µg. Viral titers in the supernatant were determined by plaque assay. B) Graph indicates DENV infection titers at 24 h pi. MCF7 cells were treated with siRNA specific to *ESR1* and scrambled siRNA as a control (labeled as NTC (non targeted control). ** p-value<0.01 ***p-value<0.001 ****p-value<0.0001. C) Graph indicated knockdown efficiency determined at mRNA level by qRT-PCR at 48 h post transfection. At 48 h post transfection, cells were infected with DENV and Cipa was added after viral adsorption. D) Boxplots with same labels have similar mean values and dissimilar labels have different mean values i.e both the boxplots with label "a" have same mean values while the box plots with labels (a, b, c) differ significantly with each other (P value<0.01 Anova test), thus signifying that non targeted MCF7 cells treated with Cipa show significant difference (higher inhibition) than targeted MCF7 cells treated with the same concentration of Cipa. Tukey test details in supplementary figure 11.

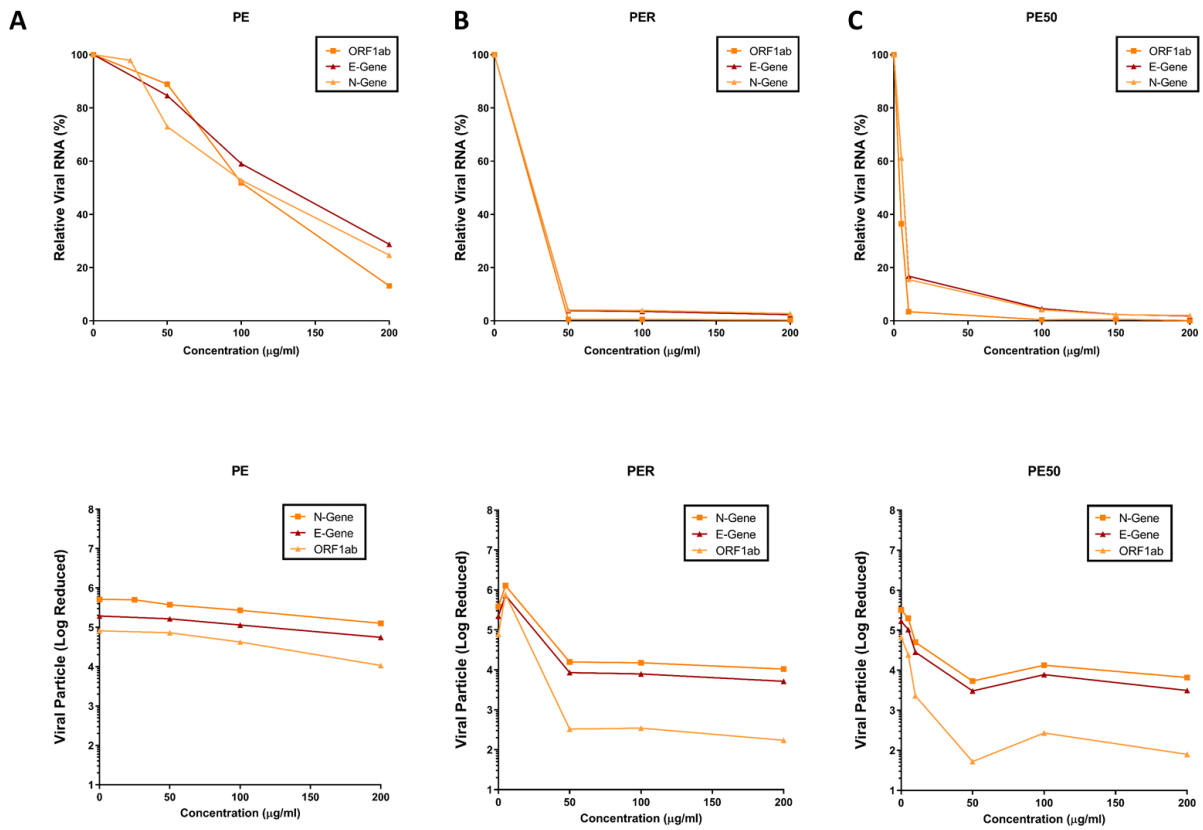

Figure 5: Whole plant aqueous extract (PE), hydro-alcoholic extracts (PE50) and root extract (PER) of Cipa inhibit SARS-COV-2 in vitro: A) Relative viral RNA % and Log reduction in viral particles in response to PE in vero cells at 50, 100, 150 and 200µg. B) Relative viral RNA % and Log reduction in viral particles in response to PE50 in vero cells at 50, 100, 150 and 200µg. C) Relative viral RNA % and Log reduction in viral particles in response to PE50 in vero cells at 50, 100, 150 and 200µg. The viral particles were calculated using quantitative PCR of N, E and ORF-1ab viral genes.

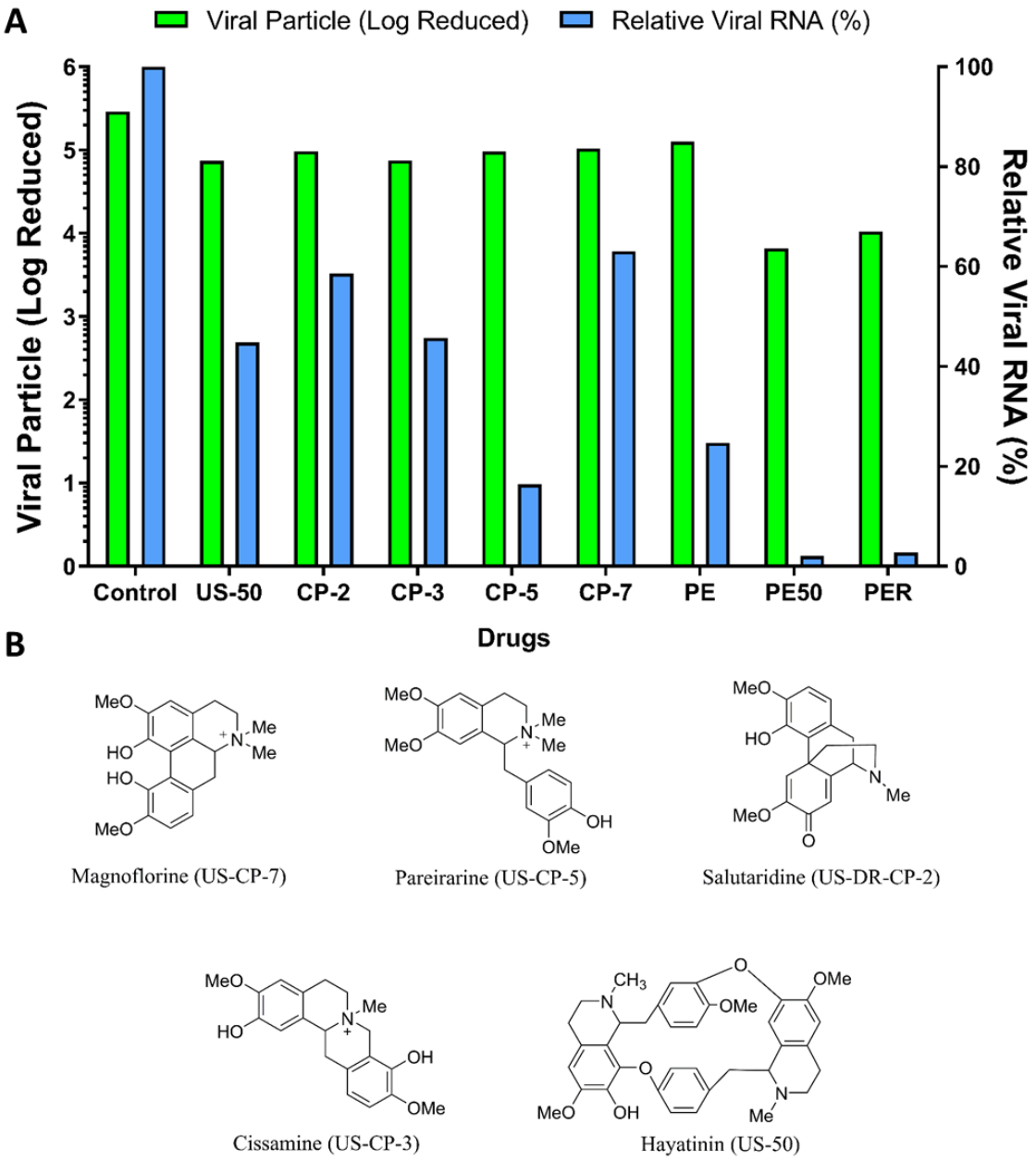

Figure 6: Cipa constituent compounds show viral reduction: A) Cipa constituents inhibit sars-cov-2 viral titers, CP-2 Salutaridine, CP-3 Cissamine, CP-5 pareirarine, CP-7 Magnoflorine, PE aqueous extract, PE50 50% hydroalcoholic extract and PER root extract. B) Chemical structures of the Cipa constituents for which the anti-SARS CoV2 activity was tested. Cissamine and Magniflorine form the major percentage of total alkaloids. Both the compounds can potentially bind ERα (Table S1).

Table 1: Cipa constituent compounds, their minimum and maximum binding energies with ER-alpha, the binding cluster each fall into (full table in supplementary)

DRUG NAME	Minimum Binding Energy(kcal/mole)	Maximum Binding Energy (kcal/mole)	Cluster
Sepeerine	-10.2	-5.8	
17-beta-estradiol (Control)	-10.1		1
Neolitsine	-9.6	-5.5	1
Oxoeletefine	-9.6	-4.7	1
Cycleanine	-9.5	-7.5	1
Liriodenine	-9.5	-5.9	1
Pareitropone	-9.4	-5.2	1
Tamoxifen (Control)	-9.2		1
Pronuciferine	-9.1	-4.8	1
Bulbocapnine	-9	-5.4	1
Cissaglaberrimine	-9	-5.7	1
Grandirubrine	-8.8	-4.9	1
Quercetin	-8.8	-5.4	1

Table 2: Amounts (mg/g) of compounds quantified in different samples of *C. pareira*

S. No.	**Samples**	**Magnoflorine** (US-CP-7) **(1)**	**Pareirarine (2)**	**Salutaridine** (US-DR-CP-2) **(3)**	**Cissamine** (US-CP-3) **(4)**	**Hayatinine** (US-50) **(5)**	**Total alkaloids**
1.	USCPWP-PE-50	12.9	5.4	NQ	18.6	9.5	46.4
2.	USCPR-PE-R	3.5	1.6	NQ	6.0	1.8	12.9
3.	USCP-PE	NQ	NQ	NQ	3.3	NQ	3.3
4.	USCP-PE-EF	NQ	7.6	NQ	8.0	NQ	15.6
5.	USCP-PE-BF	NQ	10.3	NQ	1.7	NQ	12.0